CrossMark

REVIEW PAPER

The mechanical behavior of nanoscale metallic multilayers: A survey

Q. Zhou[1] · J. Y. Xie[1] · F. Wang[2] · P. Huang[1] · K. W. Xu[1] · T. J. Lu[2]

Abstract The mechanical behavior of nanoscale metallic multilayers (NMMs) has attracted much attention from both scientific and practical views. Compared with their monolithic counterparts, the large number of interfaces existing in the NMMs dictates the unique behavior of this special class of structural composite materials. While there have been a number of reviews on the mechanical mechanism of microlaminates, the rapid development of nanotechnology brought a pressing need for an overview focusing exclusively on a property-based definition of the NMMs, especially their size-dependent microstructure and mechanical performance. This article attempts to provide a comprehensive and up-to-date review on the microstructure, mechanical property and plastic deformation physics of NMMs. We hope this review could accomplish two purposes: (1) introducing the basic concepts of scaling and dimensional analysis to scientists and engineers working on NMM systems, and (2) providing a better understanding of interface behavior and the exceptional qualities the interfaces in NMMs display at atomic scale.

Keywords Multilayer · Interface · Microstructure · Mechanical behavior

✉ F. Wang
  wangfei@mail.xjtu.edu.cn

✉ T. J. Lu
  tjlu@mail.xjtu.edu.cn

[1] State-Key Laboratory for Mechanical Behavior of Material, Xi'an Jiaotong University, Xi'an 710049, China

[2] State-Key Laboratory for Mechanical Structure Strength and Vibration, Xi'an Jiaotong University, Xi'an 710049, China

1 Introduction

Nanoscale metallic multilayer (NMM) films, consisting of two or three thin alternating metallic laminated phases with nanoscale dimensions, are a special class of nanoscale composite materials. In micromechanical devices, NMMs can play a leading role due to their desirable mechanical properties, such as order-of-magnitude increase in strength [1–4], increased ductility and fracture toughness [5–8], resistance to radiation damage [9–12], resistance to shock damage [13,14], and thermal stability [15–17], as well as better electrical and magnetic responses [18–20]. As materials scientists, one of the most basic concepts we learn is that due to the prevalence of defects, the theoretical strength of a given material is rarely realized. We have long accepted this as a fact of life when dealing with real materials. However, it has been established that the yield strength of an NMM composite can approach one half to one third of the theoretical strength limit $\mu/30$, μ being the shear modulus of its constituent metal, reaching GPa level [3]. As a result, an essential concept evolving from the mechanical behavior of the NMM composite is that unlike bulk composites that follow the rule-of-mixtures design philosophy, the volume fraction of its constituent phase is no longer a key parameter. Rather, it is the density and interfacial structure that control the strength and fracture of NMM films. In particular, the well-defined, near continuous NMM films provide essential conditions for accurate understanding and characterization of relevant interfacial structure and properties. As the idea of interface engineering has existed in various communities for many years, helpful for the design of high performance multilayer thin films and nanostructured composites, the main focus of this article is placed upon recent efforts in this field, covering (interfacial) microstructure,

mechanical properties, and plastic deformation mechanisms of NMMs.

2 Microstructure

2.1 Synthesis

NMMs with high interfacial content may be fabricated via bottom-up, near-equilibrium, thermodynamic techniques such as physical vapor deposition (PVD) and electrodeposition (ED) of two different metals that alternate many times, starting with a suitable substrate, until a desired thickness is reached. Different fabrication methods may exert different effects on the structure of the resulting multilayer, including control of scale, crystallographic texture, and residual stresses in the as-fabricated system.

PVD, using such tools as e-beam evaporation or magnetron sputtering, is the most commonly applied approach to fabricate two-dimensional (2D) planar nanocomposites having controllable phase sizes down to nanoscale as well as high thermal stabilities. It relies on physical mechanisms to produce source atoms in the gaseous state, which are then deposited onto a substrate in the form of 2D planar composites consisting of an alternating stack of two different metals. In the case of PVD-deposited multilayers, the interface, across which the metals are immiscible, can be relatively chemically sharp and ordered, as shown in Fig. 1a [5], which is consistent with molecular dynamics (MD) simulations [9,21]. Epitaxy and interface character are thermodynamically driven, defined by minimization of the energy associated with growth processes under a known set of deposition conditions, such as temperature, substrate, and deposition rate [22]. PVD is more commonly used for two main reasons: (1) it is not limited to particular materials;

(2) growth-induced residual stresses and flaws/porosity are minimized.

However, for NMMs fabrication, PVD is relatively slow compared to other methods and thus the resulting overall multilayer thickness is limited. Figure 1b shows a magnetron sputtered Ag/W multilayer with an individual Ag layer thickness of 20 nm [23], where the waviness and broken interface structure is attributed to an island growth phenomenon. Under non-equilibrium conditions, the growth is dominated by limitations to the mobility of deposited atoms, such as surface diffusion, Ehrlich–Schwoebel (ES) effect and deposition rate [24–26]. Two competitive mechanisms—roughening and smoothing—have been proposed to explain the morphological evolution (e.g., waviness) in NMMs. The waviness increases with continued deposition (increasing film thickness, Fig. 1c) [27], which may be attributed to the coalescence of islands during sputtering. For instance, during the sputtering of very thin layers, individual islands would form, followed by gradual coalescence of such individual islands. Apart from film thickness, numerical simulation results also indicated that volume fraction and inhomogeneity as well as anisotropy can play important roles in morphological instabilities in NMMs [28]. Surface energy is very sensitive to surface conditions. Defects created during growth, e.g., misfit dislocations, have a strong effect on growth. As growth proceeds, however, due to lattice misfit, when the strain energy exceeds a critical value it is energetically favorable to introduce misfit dislocations. Subsequently, islands are formed to relieve the misfit strain [28]. As a consequence, layer-by-layer growth followed by island growth is preferred.

Compared to PVD, the method of ED has a lower cost and faster low-temperature deposition rate. The synthesis of films using ED has a long history, and the overall sample thickness achieved is sufficient to make self-supported foils with technical ease. In addition, it was shown in the early 1990s that ED
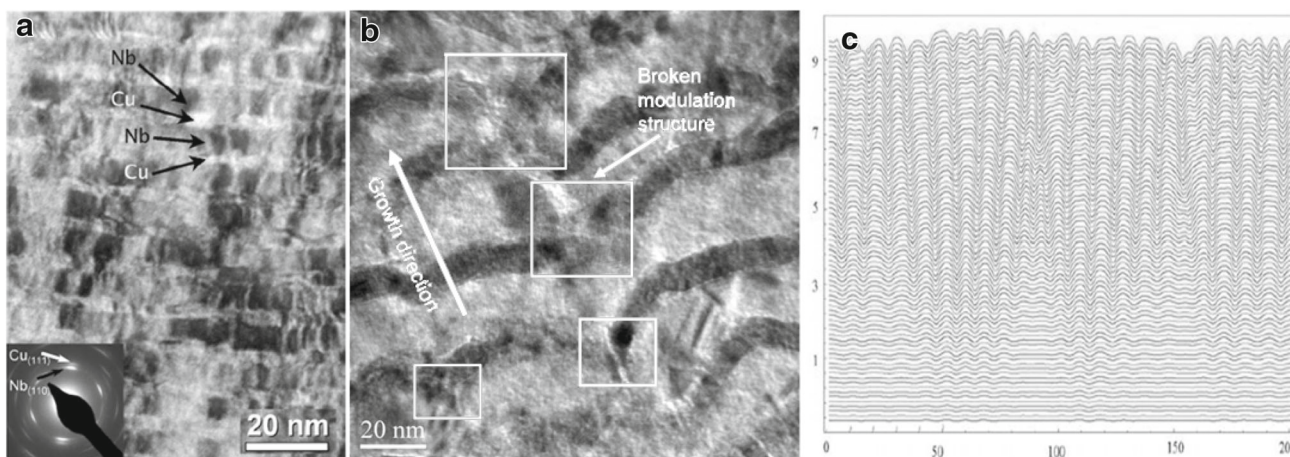

Fig. 1 a HRTEM image of sharp and ordered interfaces in a Cu–Nb PVD nanolayered composite. **b** Representative TEM image of Ag20W10, with *lines* and *boxes* used to denote the broken modulation structure in the multilayer. **c** Numerical simulation of morphology evolution. Reprinted from Refs. [5,23,27] with permission

was capable of producing multilayered magnetic nanostructures exhibiting a significant giant magnetoresistance (GMR) effect. Bakonyi and Peter [29] critically evaluated existing GMR results for various element combinations accessible to the ED technique for the preparation of multilayer films.

In spite of the relative simplicity and cost-effectiveness, ED is rarely used in practice because impurity concentration has not been well controlled and the interfaces in ED multilayers are not atomically sharp [30]. Figure 2a shows the canted microstructure of an ED Cu–Ni multilayer [31], while Fig. 2b presents the fiber morphology in a Ni81Cu19/Cu multilayer [32].

2.2 Grain morphology

Acting as a kind of polycrystalline material, the morphology of grains inside individual NMM layers should be addressed in advance. Because of different restrictions from the interfaces, three kinds of grain morphologies are common in NMMs, as shown schematically in Fig. 3 [33]. Figure 3a represents multilayers having approximately equal-axed grains, namely, the in-plane lateral grain size is close to individual layer thickness h, such as Ag/Co [34] and Ag/Cu multilayers [35]. Figure 3b represents the grain morphology of compressed grains whose in-plane grain size is several times larger than h, such as Cu/W [36] and Ag/Ni [37]. Figure 3c represents heterophase layers grown by coherent epitaxy on each other to form a superlattice columnar microstructure, such as Cu/Ni [38,39], Cu/Co [40,41], Cu/Nb [42,43], and Ni/Ru [17]. For an NMM film, surface energy between constituent layers and lattice constant relationship are two key factors dictating its grain morphologies. When surface energy difference is small, the constituent layers can form closely packed plane textures parallel to each other. Additionally, if the atomic radius ratio r_{AB} satisfies certain conditions, the multilayer film adopts epitaxial growth at the interfaces, forming a superlattice structure; see Fig. 3c–3d. Bauer [44] suggested that a superlattice structure may be characterized by surface energy mismatch Γ_{AB} and atomic radius matching r_{AB}, as:

$$\Gamma_{AB} = 2 \left| (\gamma_A - \gamma_B)/(\gamma_A + \gamma_B) \right|,$$
$$r_{AB} = a_B/a_A, \tag{1}$$

where γ is the surface energy and a is atomic radius. For $\Gamma_{AB} < 0.5$ and $r_{AB} \leq 1.00$, superlattice formation should be possible; otherwise, NMMs tend to form layered structure parallel to each other. When the in-plane grain size is much larger than the single layer thickness h (usually 8–10 times h), the NMM film may adopt a compressed grain structure in the form of columnar crystal growth within the single layer, but discontinued at the interfaces (Fig. 3b).

2.3 Thermal stability

The effect of thermal stability on grain/layer morphology has also been extensively investigated. In polycrystalline multilayer systems, the free energies of interfaces and grain boundaries will determine the relative stability of each layer as well as the overall stability of the multilayer [46]. For instance, in both the annealed Ag/Ni and Cu/Nb multilayers shown in Fig. 4 [46], deeper grooves extended into the layer to induce breakdown and pinch-off. This behavior has also been observed in a number of other NMM systems. However, Misra et al. [15] discovered that polycrystalline Cu/Nb multilayers with layer thickness greater than 35 nm exhibited long-term thermal stability at temperatures as high as 80 % of the absolute melting temperature of Cu. In the annealed films, continuity of the layered structure was maintained and the layer thickness remained unchanged. It was found that zigzag alignment of triple-point junctions (Fig. 5a) and approximate alignment of grain boundaries (Fig. 5b) were both likely to occur in NMMs. The development of zigzag alignment of triple-point junctions can effectively impede the development of grooves, contributing, therefore, to morphological stability. Nanolayers were observed to be offset by shear at zigzag-aligned triple-point junctions with equilibrium groove angles [47]. Wan et al. [48] found that zigzag microstructures experimentally observed in multilayers would form if grains in each upper layer had a relative shift less than half the in-plane grain size of the lower layer, driven by imbalance of tensions in interphase and grain boundaries. In terms of the aspect ratio of grain dimensions and the ratio of the distance between two nearest triple junctions to the in-plane grain size, Wan et al. [48] also developed stability map of layered structure in Cu/Nb systems using numerical simulations.

2.4 Atomic interface structure

The atomic interface structure is arguably the most representative internal microstructure of NMMs. Based on continuity of slip planes across an interface, interfaces in NMMs may be grouped into three categories: coherent interfaces, semi-coherent interfaces, and incoherent interfaces.

Coherent interfaces are commonly found in face-centered cubic/face-centered cubic (fcc/fcc) NMMs with cube-on-cube structure, such as Cu/Ni, where the two material layers across the interface have identical crystallographic structure and similar lattice parameters. Slip systems are nearly continuous in coherent interfaces, and there is no discontinuity between slip directions of the two layers. Therefore, dislocations can pass from one layer to another through coherent (or so-called transparent) interfaces. Nonetheless, a small lattice mismatch is usually present at coherent interfaces, leading
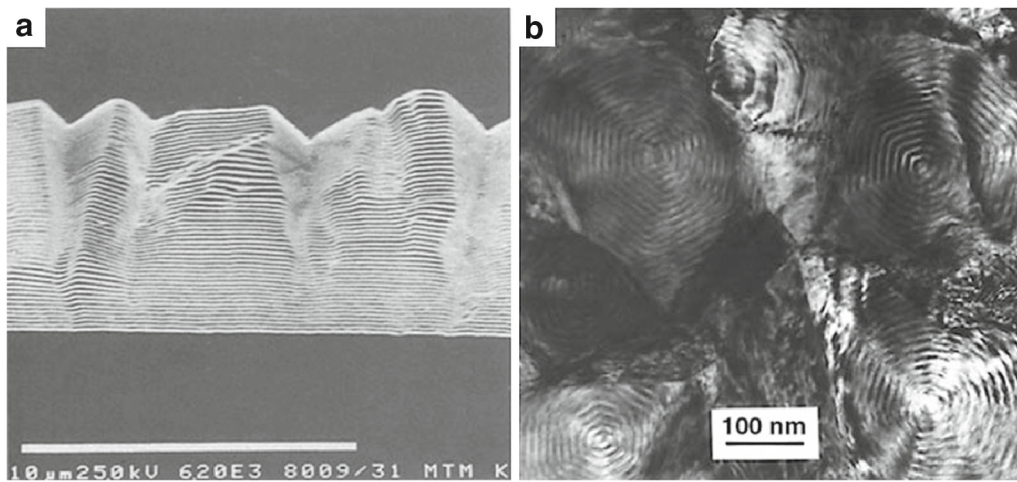
Fig. 2 **a** Cross-sectional SEM image of Cu–Ni multilayer with individual layer thickness $h = 100$ nm, showing canted effect. **b** Plane-view TEM image of Ni81Cu19 (10 nm)/Cu (1.4 nm) multilayer, showing fiber texture. Reprinted from Refs. [31,32] with permission
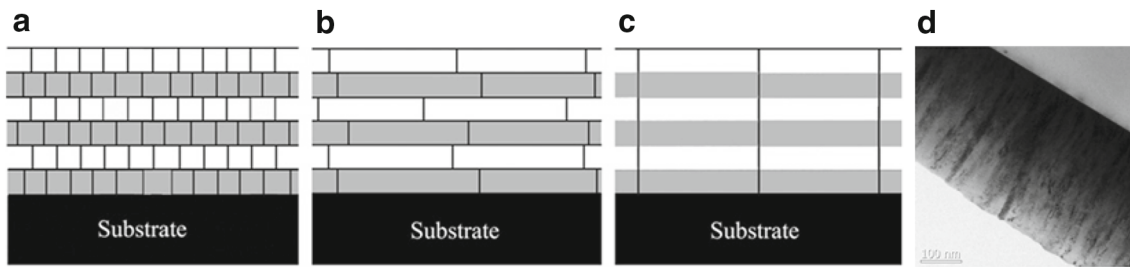

Fig. 3 Schematic of three kinds of grain morphologies: **a** Equal-axed grains. **b** Compressed grains. **c** Columnar grains. **d** Superlattice structure formed in Cu/Ru. Reprinted from Refs. [33,45] with permission

to very strong interfaces with high coherent stresses. The high coherent stresses are barriers the dislocations need to overcome to transmit to the other layers. The role played by coherent interfaces in the plastic deformation of NMMs will be discussed in more detail in Sect. 4.1.3.

Similar to coherent interfaces, the two layers of materials across a semi-coherent interface have the same crystallographic structure, but there exists a large lattice mismatch along the relaxed interface, resulting in a relative low shear resistance interface. This type of interface commonly appears
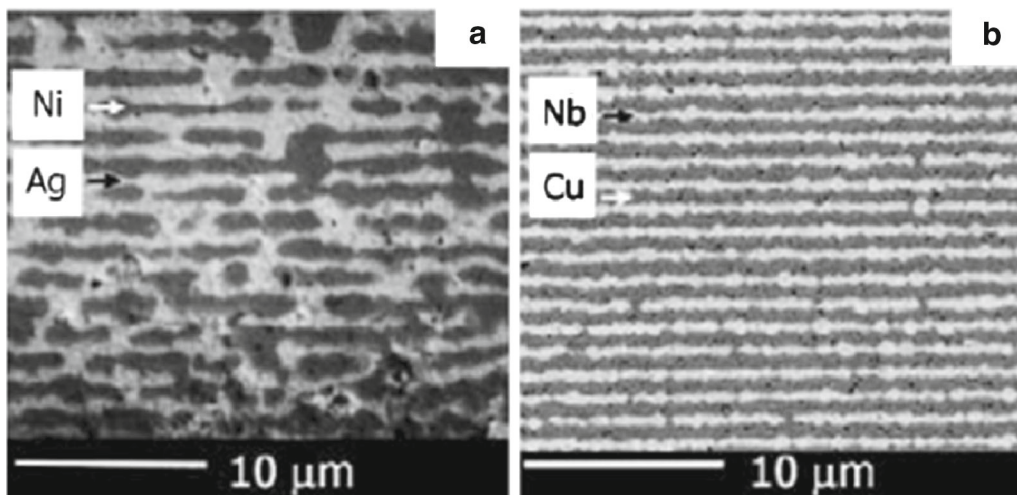

Fig. 4 SEM image of **a** Ag/Ni and **b** Cu/Nb multilayer specimens, with evident breakdown of nickel layers (*dark layers*) in **a** and pinch-off in Nb layers (*light layers*) in **b**. Reprinted from Ref. [46] with permission
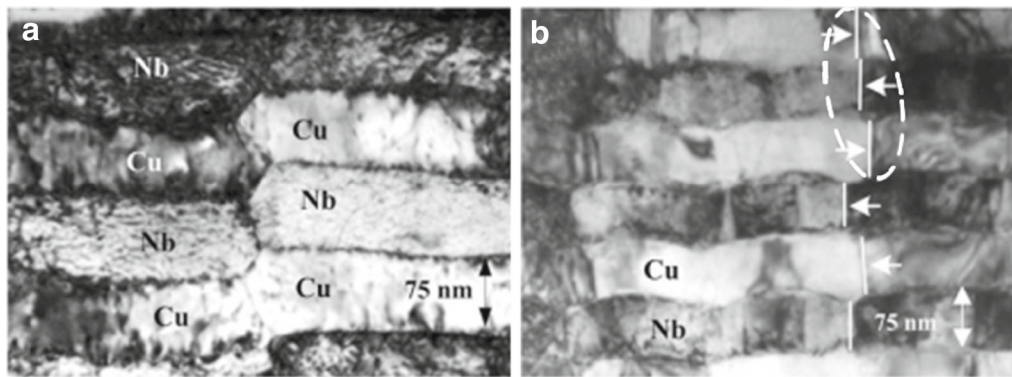
Fig. 5 Microstructures of 75 nm Cu/Nb multilayers after 1 h annealing under different temperature: **a** 1073 K and **b** 873 K. Note that the zigzag alignment of triple junctions in **a** and the approximate alignment of grain boundaries (*marked by white lines*) in **b**. Reprinted from Ref. [15] with permission

in face-centered cubic/hexagonal close-packed (fcc/hcp) NMMs. To reduce the high lattice distortion, misfit dislocations are often introduced. Therefore, in the absence of a misfit, a semi-coherent interface can easily transform into a coherent one when the layer thickness is smaller than a critical thickness h_c for coherency loss. More details about the evolution of interface structure will be presented later.

Incoherent interfaces are interfaces between layers having distinct lattice structures and high lattice mismatch, with no continuity between slip systems of adjacent layers. This type of interface is commonly found in face-centered cubic/body-centered cubic (fcc/bcc) NMMs, such as Cu/Nb [49,50]. TEM characterization (Fig. 6a) and atomistic simulations (Fig. 6b) have shown that the Cu/Nb interfaces join {111}fcc//{110}bcc planes. The {110}bcc/{111}fcc, ⟨111⟩bcc//⟨110⟩fcc interface is considered as a "self-healing" interfacial structure that satisfies the Kurdjumov–Sachs (K–S) orientation relationship. Meanwhile, the Nishiyama–Wasserman (N–W) {110}bcc∥{111}fcc, ⟨100⟩bcc//⟨110⟩fcc orientation relationship has also been reported as a low-energy interface [49], as shown in Fig. 6c. These two interfaces differ only by a rotation slightly greater than ∼5° about the interface normal {110}bcc∥{111}fcc.

Incoherent interfaces with wide and mobile misfit dislocations are less stable than semi-coherent ones. When subjected to external loading, an incoherent interface may shear easily with core spreading because of its low shear strength relative to that of the layers, as shown in Fig. 7 [51]. Wang [52,53] studied the interaction of dislocations with incoherent interfaces using atomistic simulations and found that the shear resistance of Cu–Nb interfaces is: (1) lower than the theoretical estimation of shear strength for perfect crystals, (2) strongly anisotropic, (3) spatially non-uniform, and (4) strongly dependent on the atomic structure of the interface. Although incoherent systems tend not to have large coherency stresses as coherent ones, their strengthening mechanism is more complex due to low

interfacial shear strength and the resultant trapping of mobile dislocations [54].

Relative to dislocation trapping, the nucleation of dislocations from an interface has received far more attention. For monolithic materials with large grain sizes, the dislocation sources within grain interiors are ubiquitous, operating typically at low stresses. In contrast, for multilayers with small (nanoscale) individual layer thicknesses, the dislocation sources are shifted to the interfaces, and the stresses needed to operate these sources depend on the interfacial structure and the interaction with mobile dislocations. Recently, atomic-scale modeling has been used to study dislocation nucleation from Cu/Nb PVD interfaces (either the K–S interface or the N–W interface) [55,56]. The results suggested that slight changes in interface structure could have a profound influence on which slip systems are activated in adjoining crystals.

2.5 Interface-facilitated twinning

Nanotwinned (NT) microstructures have recently received significant attention due to their impressive contributions to mechanical, thermal and electrical performances [57–60]. In terms of impeding the transmission of dislocations, twin boundaries (TBs) act in a way similar to high-angle grain boundaries (GBs), allowing NT metals to display extraordinary strength. Additionally, TBs are both efficient sinks for dislocations and active sources for mobile partial dislocations [61,62]. Hence, TBs play a vital role in the work hardening capability, strain rate sensitivity, and ductility of NT metals [63]. Within the material family of NMMs, high density stacking faults (SFs) and twins are observed even when h is reduced to 1 nm [39,64]. In the following, the role played by interface in the formation of twins in NMMs is discussed.

In general, as low stacking fault energy (SFE) is necessary for metals to form high density twins, such as 330 stainless steel, Ag and Cu, it is challenging to produce such twins
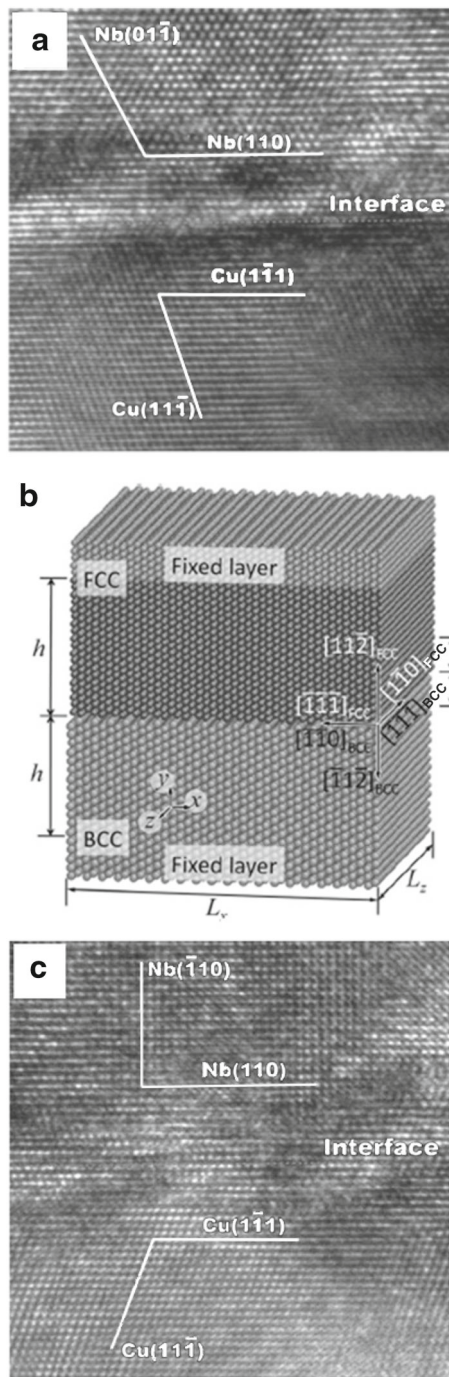
Fig. 7 Simulation result of core spreading of glide dislocation within interfaces. *Arrows* indicate the magnitudes and directions of disregistry vectors. Reprinted from Ref. [51] with permission

Fig. 6 a HRTEM image of a KS {111}fcc//{110}bcc interface in Cu–Nb NMM. **b** atomistic modeling of a Cu–Nb bilayer representing KS {111}fcc//{110}bcc interface. **c** HRTEM image of a NW {111}fcc//{110}bcc interface. Reprinted from Refs. [49,50] with permission

in high SFE metals, such as Ni and Al. The formation of high density nanotwins in systems of high SFE is another major challenge. However, fabricating NMMs is an effective technique to introduce NTs into high SFE metals, which leads to the high mechanical strength of NMMs. Coherent twin
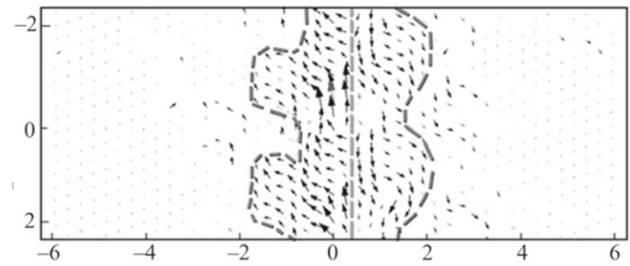
interfaces have been clearly found in epitaxial 1 nm Cu/Ni multilayers [39]; abundant SFs and coherent twins were also observed in 1 nm Ag/Al multilayers [4].

Three mechanisms are likely to be responsible for the formation of twins in high SFE metals. First, similar to SFs, coherent R3{111} and incoherent R3{112} twin boundaries (CTBs and ITBs) nucleated in a low SFE seed layer could penetrate into a high SFE layer via coherent interfaces. Additionally, once a vertically propagating TB is formed in a high SFE layer, it can often extend across many layers [65]. Second, CTBs are replicated laterally from a low SFE seed layer into a high SFE layer. Once the CTBs terminate at the layer interface, ITBs would have to nucleate inside the high SFE layer to join the variants, increasing accordingly the total system energy. Therefore, energetically, the propagation of CTBs across layer interface into a high SFE layer is more favorable than termination [38,39,64,65]. Third, the concept of misfit twin-induced alleviation of coherency stresses is less likely to account for the formation of twins in a high SFE layer [39,65].

Commonly, the driving force available to nucleate twins during the growth of NMMs stems mainly from coherent stresses. As partial dislocations must form prior to the formation of twins, shear stresses must exist to trigger the formation of partial dislocations. Take Cu/Ni as an example, atoms are typically attached to the peripherals of terraces during the process of island growth. At the free surface of Cu islands that grow epitaxially on Ni substrate, there is no stress. However, residual stresses quickly develop in Cu films when moving away from the free surface. Thus, to introduce coherency stresses in Cu, interfacial shear stress is necessary along Cu/Ni interfaces close to the free surface. This shear stress, τ, may be estimated by [66]:

$$\tau = \frac{\varepsilon E}{1 - \nu} \sqrt{\frac{E_s h_f}{2 E_f \pi x}}, \tag{2}$$

where E_s and E_f are the Young's modulus of the substrate and film, respectively, h_f is the film thickness, x is the distance from island edge, ε is the misfit strain, and b is the

Burgers vector. The high shear stress estimated at the edge of the terrace is sufficient to nucleate Shockley partials in Cu, causing subsequently the formation of fine twins during continuous growth [64].

3 Mechanical properties

3.1 Yield strength/hardness

Hardness (or, equivalently, yield strength) has been the most commonly studied mechanical property of metallic films in view of the significant progress in nanoindentation. Interest in metallic NMMs emanated initially from the order-of-magnitude increase in hardness (and yield strength) achieved by decreasing the layer thickness h [65]. (The hardness of an NMM is obtained by multiplying its tensile yield strength by 2.7 [67]). With rapid development of nanotechnology, recent attention has mainly focused on the range of $h < 100$ nm. In particular, extensive works have been conducted experimentally and theoretically on Cu/Ni [30,38,39,65,68–75] and Cu/Nb [1,5,6,42,43,69,74–78] NMMs.

In general, the strength and hardness of NMMs are influenced by layer thickness, interface orientation, interfacial structure, and fabrication method. The hardness of a NMM fabricated via electrodeposition {001} is different from that obtained with electrodeposition {111}, despite similar layer thickness, interface sharpness, and interface orientation [70,72]. Interface orientation strongly affects the hardness of a NMM system. For instance, a PVD {111} multilayer with a strong [111] Cu ∥ [111] Ni orientation relationship normal to interfaces [38] exhibits a different hardness from that of a PVD {001} multilayer having a strong cube-on-cube or [001] Cu ∥ [001] Ni orientation relationship [72]. Further, the dependence of NMM hardness upon h remains a hot topic. Figure 8 presents existing hardness (H) data for various NMM systems [79]. A variation trend similar to polycrystalline metals is observed, namely, the smaller the stronger. Discussion of the length-scale dependent strengthening mechanism is left to Sect. 4.1.

For the widely investigated Cu/X NMMs, Table 1 compares their peak hardness (H_{max}), Young's modulus mismatch (E_X/E_{Cu}), and hardness enhancement. The hardness enhancement is derived from the hardness ratio of H_{max} to the rule-of-mixture estimate (H_{rom}) from monolithic constituent films. Previously, the origin of hardness enhancement has mostly been discussed in terms of dislocation interaction with interfaces between elastically mismatched materials, and it has been postulated that the Koehler stress plays a dominant role in determining the peak strength, especially in systems with large elastic modulus mismatches [79,80]. In a multilayer system, as the line energy of a dislocation is proportional to shear modulus μ, dislocations are attracted
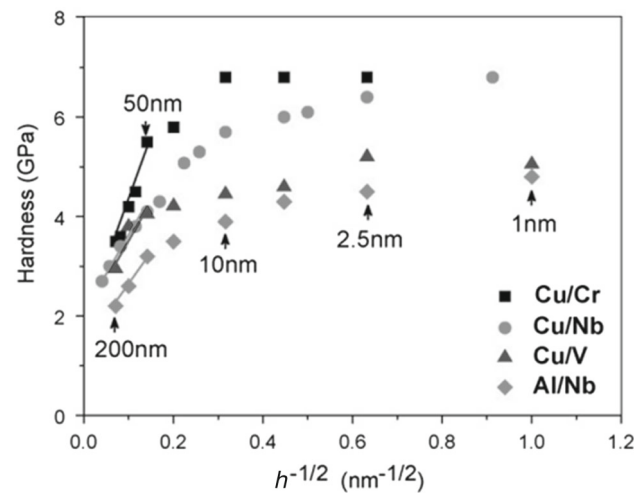

Fig. 8 Comparison of hardness versus $h^{-1/2}$ plots for various metallic multilayer systems. Reprinted from Ref. [79] with permission

to reside in low modulus layers. However, one key point that can be clearly observed from Table 1 is that hardness enhancement does not correlate with the bulk modulus of the constituent materials. For example, Cu/Au and Cu/W multilayers have similar hardness enhancement, yet their Young's modulus mismatch differs by nearly a factor of six. Accordingly, increasing E does not necessarily lead to enhanced H. More generally, it is believed that the strength and interface properties of a multilayer derive more from its interfacial structure, bonding, and defects [74,81].

3.2 Elastic modulus

As far as mechanical strength is concerned, NMMs are one of the strongest synthetic materials ever produced. Apart from significant hardness enhancement, it has been well established that significant elastic anomalies also exist for many NMM systems. For instance, the modulus values of Cu/W [36] and Cu/Nb [77] increase with decreasing h and are much higher than those of monolithic films. However, for Cu/Co [41] and Cu/Ru [86], their elastic modulus exhibits a weak dependence on h. For Ag/Ni [37], Ag/Cu [35], Ag/Nb [87], Ag/Co [88], Ni/Ru [17], and Ag/W [89], the modulus even decreases as h is reduced

For Cu/W multilayers prepared by evaporation deposition, the interfaces of Cu on W and W on Cu are asymmetrical. During the deposition process, Cu atoms with relatively high homologous temperature have greater mobility than W atoms. Thus, when Cu atoms are deposited onto a W surface, a smooth surface tends to form with relatively low surface energy. By contrast, when W atoms are deposited onto a Cu surface, the vapor atoms are incorporated epitaxially close to their arrival point owing to their low mobility, and it is difficult for them to form a smooth surface or diffuse into the

Table 1 Comparison of peak hardness, Young's modulus mismatch (E_X/E_{Cu}) and hardness enhancement H_{max}/H_{rom} for a variety of Cu/X multilayer systems

Systems (Cu/X)	Layer thickness, h (nm)	Peak hardness, H_{max} (GPa)	Elasticity mismatch E_X/E_{Cu}	H_{max}/H_{rom}	References
Cu/Ni	1.75	6.83	1.65	1.89	[38]
Cu/Au	25	2.45	0.56	1.23	[82]
Cu/Co	1	6	1.75	1.60	[40]
Cu/Fe	5	4.8	1.61	1.49	[83]
Cu/V	2.5	5.2	0.97	1.56	[79]
Cu/Cr	10	6.8	2.40	1.36	[1]
Cu/W	4	8.9	3.30	1.25	[36]
Cu/Ta	30	7.0	1.44	1.08	[84]
Cu/Zr	5	5.8	0.68	1.54	[85]
Cu/Ru	5	8.1	3.58	1.16	[86]

under layer [36]. The intermixing leads to the compression of out-of-plane interplanar spacing of the W layer, causing modulus enhancement as h is reduced. For the same reason, the enhanced modulus of fcc/fcc Cu/Nb [77] is attributed to the compressed out-of-plane interplanar spacing of fcc Nb layer.

However, although supermodulus effect (multilayer modulus much higher than those of monolithic films) exists in most multilayer systems, a drastic softening of 30 %–50 % in elastic modulus is often observed as the periodicity in a multilayer is reduced [35,37,89–91]. For example, for Cu/Nb [77], Cu atoms are probably able to penetrate into the locations of incomplete coalescence to form intermixing regions with amorphous microstructure between grain boundaries in Nb layers or at interface when h is further reduced. Further, investigation of Ag/Nb indicates that free volume in the amorphous alloy region has a negative contribution to the modulus, causing a decrease of modulus with decreasing h because more interfaces are present in the multilayer [87]. The same phenomenon is found in Cu/Cr, namely, its indentation modulus E exhibits a non-monotonic evolution with h, attaining a maximum at $h = 25$ nm [91]. This unusual variation in E is related to the competition between enhancement effect induced by compressed out-of-plane interplanar spacing of constituent layers and reduction effect associated with the formation of interfacial amorphous intermixing layers.

Another explanation proposes that the decrease of E with decreasing h is attributed to the presence of compliant interfaces [37,88]. The modulus of a multilayer may be calculated using the following equation [81]:

$$\frac{1}{E} = 2h \left(\frac{2h_i}{E_{int}} + \frac{2h - 2h_i}{E_0} \right)^{-1}, \tag{3}$$

where h_i is the interface thickness, E_{int} is the interface modulus, and E_0 is the rule of mixture value. Consequently, as the periodicity is reduced, more compliant interfaces are formed in the multilayer, causing its elastic modulus to decrease with

decreasing h. This result also indicates that there may exist interface layers whose structure is different from the intra-grain crystalline structure, and these interface layers may affect the plastic deformation mechanism of NMMs.

3.3 Ductility

Ductility data for NMM films are at present limited since nanoindentation has been the primary mechanical test method. Most of the available engineering strain data are obtained from tensile [78,92] and micropillar compression [5,93] tests. Usually, tensile tests generate much smaller values, reflecting that tensile failure often involves crack nucleation from edge defects in the thin films. In general, the strength and ductility of a multilayer are mutually exclusive, i.e., the ductility of NMMs drops with decreasing h, exhibiting a reverse trend to the strength [5,8,92].

In contrast, compression failure often involves shear localization in equiaxed samples machined from a NMM film and loaded perpendicular to its interfaces [94]. Experimental results on the ductility of NMMs obtained by the Los Alamos group [5,94] with nanoindentation testing showed that compressed Cu/Nb NMMs pillars exhibited a significant ductility. However, the ductility decreased from 36 % to 25 % when h was reduced from 40 to 5 nm. Further, rolling studies on nanoscale Cu/Nb multilayers [95,96] demonstrated rolling strains of >60 % with no material failure. However, for Cu/Nb multilayers, Misra et al. [97] showed that the rolling strain to fracture decreased rapidly when h was reduced to less than about 30 nm. Obviously, how to improve the ductility of NMMs has become a critical issue for optimized materials selection, design and fabrication.

3.4 Fracture behavior

The selection and design of high-performance NMMs is driven by optimized combinations of mechanical properties

and requirements for predictable and non-catastrophic failure in service. Therefore, understanding the fracture mechanisms of an NMM system is critical for understanding how it will perform in service. Ultimately, the exploitation of an NMM multilayer in engineering applications depends on its strength and fracture toughness. However, so far, the superior strength of NMMs is achieved at the expense of low ductility and fracture toughness, which limit considerably their practical applications. Similar to the ductility of NMMs, such a contradictory trend may also be attributed to the increased propensity of strain localization as the length scale (layer thickness) is decreased.

The fracture behavior of an A/B NMM system consisting of alternating ductile (A) and brittle (B) layers may be described using a micromechanics model [8,98,99]. In this model, the deformation capability of the ductile A layer is quantitatively evaluated by deriving an equilibrium number of dislocations that can be accumulated in this layer. The model assumes that once a crack is nucleated, a pre-existing microcrack will easily propagate to form an opening crack throughout the whole B layer and reach the A/B interface, with high stress concentration near the crack tips. Crack propagation is then a function of applied stress intensity, crack-tip shielding due to plastic deformation, and ability to accommodate crack-tip dislocation activity without crack advance [8]. If the stress intensity near the crack tip is sufficiently large, edge dislocations from the A layer can be generated at the crack tip, so that the crack can induce plastic shear through emission of edge dislocations from the crack tip (Fig. 9a). Dislocations thus emitted may have two effects. Firstly, they blunt the crack tip and reduce stress concentration at the crack tip. Therefore, the fracture progress is suppressed and it is more difficult to reach the cohesive strength of the A layer. The free-standing layer in front of the opening crack could thence be easily deformed via dislocation gliding across the whole layer. Secondly, when these dislocations move to an interface, a back stress is sent to the crack tip. The back stress will impede further dislocation emission, promoting, therefore, the fracture progress. At a given load level, the equilibrium number of dislocations n is [8,98]:

$$n = \frac{4\pi(1-v)}{\ln\left(\widetilde{h}/\widetilde{r}\right)}\left(\frac{\widetilde{K}_{app}\sqrt{\widetilde{h}}}{A\sqrt{2\pi}}\sin\varphi\cos\frac{\varphi}{2} - \widetilde{\gamma}\right), \qquad (4)$$

where $\varphi = 45°$ is the inclination angle of slip plane to the interface, $A \approx 1$, $\bar{r} = 2.7r_0/b$, r_0 is the effective core radius in A, $K_{app} = 1.12\sigma_{app}\sqrt{\pi h}$ is the far field mode I stress intensity [99], $h_\varphi = h/\sin\varphi$, and γ is the surface energy, respectively. For convenience, the following non-dimensional parameters have been introduced:

$$\widetilde{K} = \frac{K_{app}}{\mu\sqrt{b}}, \quad \widetilde{h} = \frac{h_\varphi}{b}, \quad \widetilde{\gamma} = \frac{\gamma}{\mu b}, \qquad (5)$$
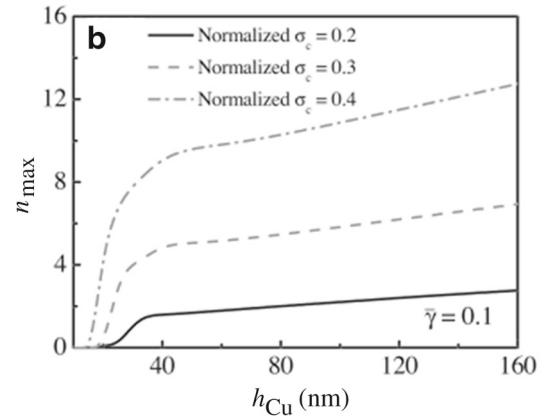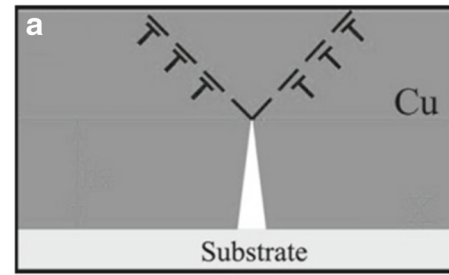

Fig. 9 **a** Sketch of dislocation emitted from interface in Cu/X NMMs. **b** predicted n_{max} plotted as a function of h. Reprinted from Ref. [8] with permission

where μ is the shear modulus. The stress at the blunted crack tip, $\widetilde{\sigma}_{tip}$, is thence related to n and K_{app} as,

$$\widetilde{\sigma}_{rip}\sqrt{n} = 2\sqrt{\frac{2}{\pi}}\widetilde{K}_{app}\left[1 - \frac{3\left(\sin\varphi\cos\frac{\varphi}{2}\right)^2}{\ln\left(\widetilde{h}/\widetilde{r}\right)}\right]$$
$$+ \frac{12A}{\sqrt{h}\ln\left(\widetilde{h}/\widetilde{r}\right)}\widetilde{\gamma}\sin\varphi\cos\frac{\varphi}{2}. \qquad (6)$$

When the stress at the crack tip reaches the fracture stress σ_c of the material ($\widetilde{\sigma}_{tip} = \widetilde{\sigma}_c$), the crack will propagate to the A layer so that a channel crack is formed. The maximum number (n_{max}) of equilibrium dislocations emitted from the crack tip prior to cleavage in the A layer can be obtained from Eqs. (4) and (6). In addition, the far-field applied stress intensity under this condition is the fracture toughness of the NMM multilayer, which can be obtained from $\widetilde{K}_{IC} = \widetilde{K}_{app}$.

The predicted n_{max} for Cu/Nb (see Fig. 9b) exhibits apparently a size effect [8], that is, with h increasing from 5 to 25 nm, n_{max} increases sharply. As a larger n_{max} implies better plastic deformation capability, the Cu layers become more ductile, hindering, therefore, crack propagation in the brittle Nb layers. The propagation of a microcrack in the Nb layer mainly depends on the far field mode I stress intensity (K) ahead of the microcrack, which scales as $h^{0.5}$[100]. As a result, when h is increased, K increases so that both the ductility and fracture toughness (K_{IC}) of the NMM decrease.
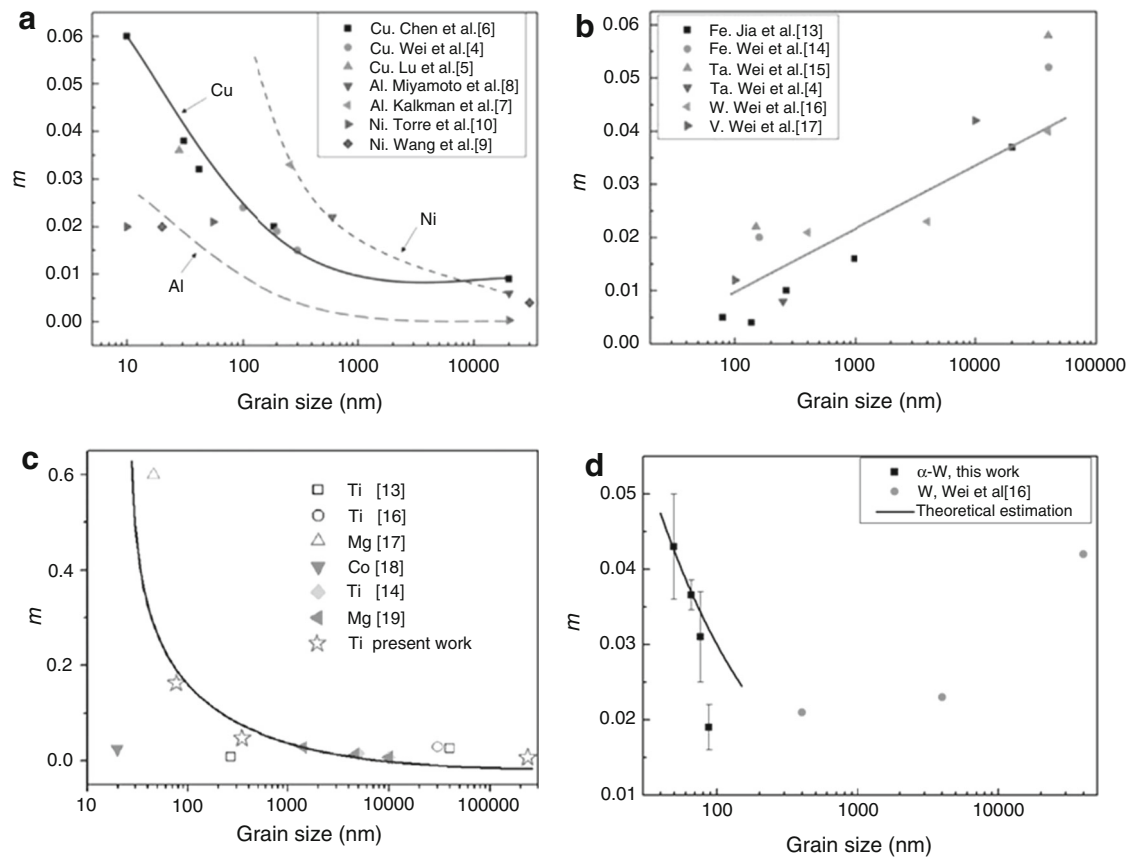
Fig. 10 Strain rate sensitivity of **a** fcc, **b** bcc and **c** hcp metals summarized using data from existing literature. **d** Strain rate sensitivity of bcc W at a grain size smaller than 100 nm. Reprinted from Refs. [102,106] with permission

Meanwhile, a larger K indicates that the microcrack can propagate more easily to form an opening crack, confirming the prediction [8] that at the critical condition of h_{cri}, a transition in fracture mode (from opening to shear) may occur. These results suggest that rather than the strengthening mechanism, the constraint effect imposed by the ductile A layer on the brittle B layer is the dominant factor that controls the modulation period and modulation ratio dependent fracture mode in A/B NMM systems [101].

3.5 Strain rate sensitivity

Strain rate sensitivity (m) is a crucial parameter that could shed light on the rate controlling mechanisms in of NMMs during plastic deformation. It describes the dependence of flow strength σ on the rate of strain $\dot{\varepsilon}$ as [102]:

$$m = \frac{\partial \ln \sigma}{\partial \ln \dot{\varepsilon}} = \frac{\sqrt{3}k_{\mathrm{B}}T}{V^*\sigma}, \tag{7}$$

where V^* is the activation volume. Equation (7) suggests that sampling volume is involved in dislocation activities, the latter also responsible for NMM plastic deformation.

The variation trends of strain rate sensitivity in NMMs with h are complex due to the coexistence of two different constituent phases. Before clarifying the rate-dependent deformation characteristics of NMMs, the strain rate sensitivity of single-phase nanoscrystalline (NC) metals needs to be addressed. Experimentally, it has been found that m is highly sensitive to the average grain size (d) or nanotwin thickness [103–105]. It has also been found that the size dependence of rate-sensitive parameters is closely related to the lattice structure of NC metals. Figure 10a [102] shows that m for several fcc metals increases monotonically when d is decreased, with $m > 0.1$ for NC fcc metals. In contrast, Fig. 10b [102] shows that m for bcc metals has the opposite dependence on grain size, with $m < 0.1$ for NC bcc metals. However, Fig. 10c indicates that hcp metals have a similar trend as that of NC fcc metals [106].

For multilayer thin films, the fundamental questions about strain rate sensitivity (m) are [107]: (1) competition or cooperation effect between the two constituent phases (e.g., fcc vs. bcc) at nanoscale, given that they have radically different variation trends of m with grain size d, as compared in Fig. 10; (2) influence of dissimilar interface structure (e.g., coherent vs. incoherent) in NMMs on m; (3) possibility of other char-

acteristic microstructures, such as grain size or twins, that may have an effect equal to or greater than that of the interface.

First, consider the influence of constituent layers, i.e., fcc versus bcc, or fcc versus hcp. With the NMMs taken simply as a composite, their properties are affected by each constituent phase. A rate jump compression was used by Carpenter et al. [71] test to study rate effects in Cu–Ni multilayers. Obtained room-temperature values of m varied from 0.013 to 0.020 as the compressive stress was increased from 660 to 1800 MPa. These m values are similar to those for NC fcc metals. The same trend (m decreasing with increasing h) was also detected in Ag/W [23]. Results presented in Fig. 10b show that the bcc W has an opposite dependence of m on d; however, as the grain size dropped below a critical value (e.g. 100 nm for W), elevated m was observed due to GB-related deformation mechanisms (Fig. 10d [102]). As the grain sizes in both Ag and W layers have been found to scale positively with h [23], the strain rate sensitivity of the Ag/W NMMs should decrease with increasing h when h falls within the nano regime. This is because enlarged grain size in Ag and W layers will lead to reduced strain rate sensitivity in Ag/W multilayers, and the plasticity is shared by both Ag and W phases. However, it is interesting to notice that the m values of Ag/W multilayers with h larger than 50 nm are almost equal to that of Ag film since plasticity is localized in the soft fcc Ag layer. In comparison, for Cu/Nb multilayer with $h = 10$ nm [42], m is equal to that of bcc Nb film. The rate of climb in Cu layers will be much larger than that in the Nb layers. Thus, the resistive force induced by increasing strain is easier to be released by the process of dislocation annihilation, assisted by climb in Cu layers. As a result, the majority of the extra load required to overcome strain hardening in a Cu/Nb multilayer is taken up by Nb layers. The multilayer exhibits, therefore, similar rate-controlling characteristic of the Nb film.

Second, to clarify further the creep mechanisms during the indentation process in NMMs, Zhu et al. [38,41,108] carried out a series of room temperature indentation creep testing to measure the strain rate sensitivity and creep stress exponent n^*. As for indentation creep with a self-similar indenter, n^* may be extracted through the following relation [109]:

$$-n^* \ln H(t) = \ln B - \frac{Q}{RT} + \ln t, \qquad (8)$$

where $H(t)$ is the instantaneous hardness, t is the time for load holding, B is a dimensional scale constant and Q is the activation energy. In general, the stress exponent n^* should scale inversely with m. For Cu/Ni [38] and Cu/Co [41] with coherent interfaces, the stress exponent n^* was found to increase with decreasing h. As the coherent superlattice structure forms when h is reduced, the density of edge

dislocations settled at the interfaces declines, thus reducing the effective diffusion paths provided by the interfaces. Consequently, the stress exponent increases and the strain rate sensitivity decreases with decreasing h. In contrast, for Ag/Fe with incoherent interfaces [108], as h is reduced, a monotone drop in stress exponent and increase in strain rate sensitivity is observed. As a creep process is typically dominated by the mechanism of dislocation glide-climb, the increased fraction of grain boundaries and incoherent interfaces provides effective diffusion paths for creep climb because grain boundaries and incoherent interfaces can be the source to emit and absorb dislocations [110]. As a result, it is not surprising that the creep process exhibits a higher strain rate sensitivity when h is reduced.

Third, grain size as well as twin spacing play important roles in controlling the strain rate sensitivity of NMMs. Consider, for instance, the influence of grain size in both A and B constituent layers on the strain rate sensitivity of A/B multilayers. Given the contribution from GB, the effective rule of mixtures (ROM) for evaluating the strain rate sensitivity of two phase (A and B) materials may be modified. On the other hand, the dragging force that the interfaces exert on a single slip dislocation increases rapidly with decreasing periodicity, as layer thickness and grain size are both reduced. The viscous glide velocity then falls below the dislocation climb velocity, so that viscous glide will dictate the rate-controlling process and the value of m. In Ag/Cu multilayers, a transition of creep deformation mechanism from dislocation movement to grain boundary sliding occurs as h is less than 15 nm [35]. In Ag/Ni multilayers, the dependence of creep rate on layer thickness reveals that grain boundary deformation is more dominant for $h < 4$ nm [111]. In this case, when the layer thickness is small enough, the strain rate sensitivity and creep rate of the multilayer should always increase with decreasing h, independent of interface structure [38,41]. Apart from grain size, the decreasing rate sensitivity found in Cu/Zr and Cu/Cr [107] is potentially a result of decreasing twin fraction in Cu at small h. In addition, the non-monotonic evolution of m with h observed in Cu/X multilayers may be explained by a competition between monotonically increased interface density and decreased twin boundary density [112].

4 Plastic deformation

4.1 Length-scale-dependent deformation mechanisms

NMM materials are rather suitable for fundamental studies of length scale effects, in the micrometer to nanometer thickness range, on deformation mechanisms of metallic nanocomposites. Built upon previous experimental and theoretical studies, Misra et al. [76] produced Fig. 11 to summarize deformation regimes in metallic multilayer thin films hav-
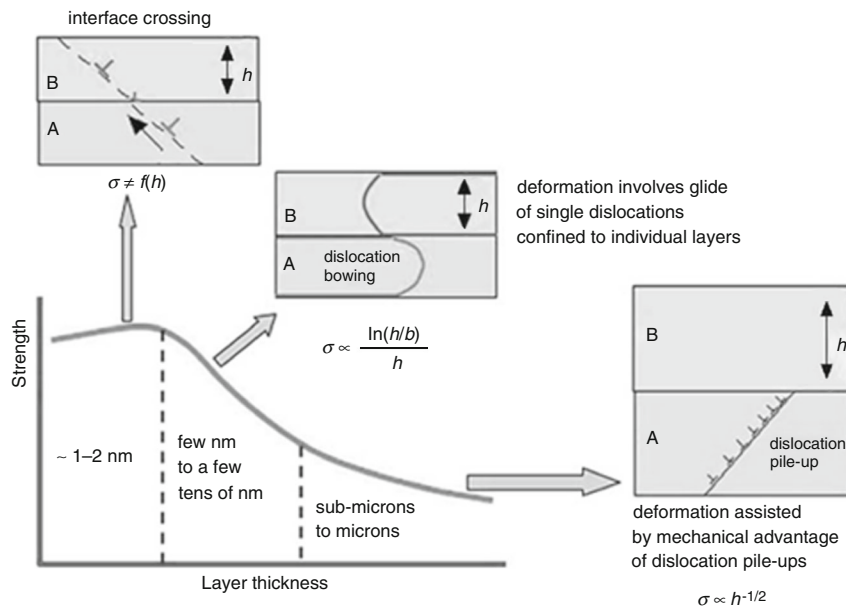
Fig. 11 Deformation mechanisms active at different length scales. Reprinted from Ref. [76] with permission

ing varying individual layer thickness h. Under a constant modulation ratio of 1, the hardness/strength curve of NMMs usually exhibits three distinct regions: Hall–Petch (H–P), single dislocation, and interface crossing.

4.1.1 Hall–Petch regime

At sub-micrometer to micron length scales, the applicability of the classical H–P strengthening relation is built upon the premise that dislocations piling up against an interface are responsible for the yielding behavior of lamellar metals [73,113]. The success of the H–P relation in describing the strength of many polycrystalline materials suggests that its origin is very fundamental, and that similar behavior should be observed in multilayers (including NMMs). Thus, according to the H–P relation, the yield stress σ_{ys} of a NMM multilayer is related to its layer thickness h as [76]:

$$\sigma_{ys} = \sigma_0 + kh^{-1/2}. \tag{9}$$

Figure 7 demonstrates that a linear fit to the hardness of NMMs at coarse length scales is consistent with the H–P theory. In this theory, the interface boundary is assumed to act as an obstacle to dislocation motion. Dislocations emitted from a source move along the same slip plane and propagate towards the interface. Once the lead dislocation is stopped by the interface, the trailing dislocations stop behind it due to mutual repulsion, causing dislocation pileup at the interface. The number N of dislocations in a pileup subjected to an applied shear stress τ scales with the distance L between the source and obstacle, as [9]:

$$N = \frac{\pi L(1-v)(\tau-\tau_0)}{\mu b}, \tag{10}$$

where v and τ_0 are the Poisson ratio and lattice friction stress, respectively. When the stress concentration at the pileup eventually exceeds the interface barrier, the NMM plastically yields. Since the H–P slope represents the strength (τ_{int}) of the interface barrier, the peak strength of the NMM may be estimated from the measured slope by [76]:

$$\tau_{int} = \frac{k^2 \pi(1-v)}{\mu b}. \tag{11}$$

By multiplying τ_{int} with the Taylor factor, theoretical estimates of the ultimate peak strength may be obtained for NMMs.

4.1.2 Single-dislocation regime

When the layer thickness h is further reduced, the H–P effect on strength levels off in the vicinity of $h \sim 50$ nm even though the strength continues to increase with decreasing h [79]. This breakdown occurs, in part, because Eq. (10) treats the number of dislocations N as a continuum, valid only when $N \gg 1$. In fact, for $d \sim \mu$ m or larger, dislocation sources within grain interiors are ubiquitous and operate at low stresses. When h approaches several nm, slip occurs by motion of single dislocations (as opposite to continuum-scale pileups) and the interfaces become the controlling parameter in plastic deformation [114]. Under such conditions, dislocation sources shift to the interfaces and the stress to operate them, which depends on the h-dependent interfacial structure. The
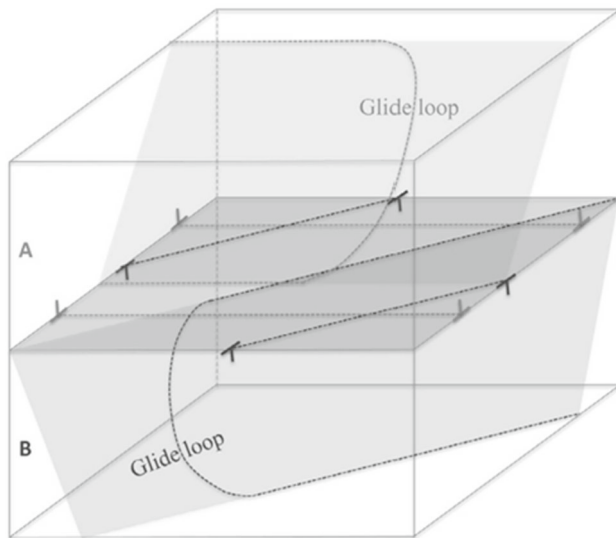
Fig. 12 Schematic of confined layer slip mechanism in multilayer structures. Dislocation loops glide individually in each layer and deposit dislocations in the interface plane. Reprinted from Ref. [116] with permission

strengthening mechanism has been described [76,115,116] as an effect of confined layer slip (CLS) of single-dislocation loops within the confined geometry of NMM, as shown in Fig. 12 [116]. Experimentally, these loops are shown to originate from existing threading dislocations, from interfaces, and from interactions with other dislocations [56,115–118].

Based on the CLS model [76], plastic yielding would occur when dislocations are curved into a semicircle within the confined geometry of a constituent layer. Concerning dislocation core spreading, residual interface stress, and interaction between gliding dislocations with stress fields arising from misfit dislocation arrays deposited at the interface, the refined CLS is generally believed to be an excellent descriptor for strength, given as [76]:

$$\sigma_{\text{CLS}} = \frac{M\mu b}{8\pi h_\varphi}\left(\frac{4-v}{1-v}\right)\ln\left(\frac{\alpha h_\varphi}{b}\right) - \frac{f}{h} + \frac{\mu b}{s(1-v)}, \quad (12)$$

where $h_\varphi = h/\sin\varphi$ is the layer thickness measured parallel to the glide plane. φ is the angle between the slip plane and the interface. α is the core cut-off parameter. f is the characteristic interface stress of the multilayer. $s = 2bm_0/\varepsilon_0$ is the mean spacing between misfit dislocations deposited at the interface, m_0 being the strain resolution factor. And ε_0 is the in-plane plastic strain [76]. Attention should be paid to the interface stress (f) that arises from elastic deformation of the interfacial region. Under tensile loading parallel to the interface, the applied stress must also do work against interface stress, which is usually negative for metal systems. However, for indentation hardness testing, the interface stress would assist the applied stress [76].

Equation (12) provides a good fit to existing strength data of most NMM systems as h is reduced from tens of nanometers to several nanometers. However, at very small h (less than core cut-off dimension), the equation used to calculate the dislocation self-energy is no longer valid because the log term in the equation becomes negative, leading to negative values of the CLS stress. Note that the model predicts increasing strength with decreasing h, while experimental data indicate that a peak strength is achieved at $h \sim 1$–2 nm and, as h is reduced below 1 nm, a drop in strength may occur as well. Consequently, the CLS model is not applicable when h is less than about 2 nm.

4.1.3 Interface-crossing regime

Figure 8 indicates that when h is sufficiently small, its effect on strength levels off, until a decrease in strength is observed, which is popularly called the inverse H–P effect, as observed in bulk nanocrystalline metals. Within this regime, the mechanism of interface crossing or dislocation transmission controls the strength. The saturation or plateau in strength has been attributed to the stress exceeding the threshold needed for interfacial transmission [76,119]. In the interface-crossing regime, it has been found that the strength is predominantly related to interface structure barriers between two constituent layers. Both coherent and incoherent interfaces can cause significant strength enhancement for a multilayer system relative to its bulk counterparts. However, experiments show that the strengthening mechanisms for systems having coherent interfaces are different from those with incoherent interfaces [120–122]. In the following sections, the mechanical properties of multilayer thin films arising from different structures of interfaces and their interaction with mobile dislocations are discussed in sequence.

For coherent interfaces such as epitaxial Cu/Ni, geometrical barriers to transmission are absent, in the sense that a dislocation can glide across an interface with ease, leaving simply a step at the interface. Despite this, the strength of a multilayer thin film with coherent interfaces is larger than those of its bulk materials. Potential mechanisms proposed to interpret this anomalous interface effect include image stress strengthening [79,80,123], coherent stress strengthening [74,124,125], misfit dislocations strengthening [74,76, 126], chemical mismatch strengthening [4,40,74], and solid solution strengthening [127]. More precisely, with mechanistic underpinnings of the interface-dependent strengthening mechanism, the interface strength barrier resistance τ_{int} may be expressed as [40]:

$$\tau_{\text{int}} = \tau_{\text{K}} + \tau_{\text{Ke}} + \tau_{\text{coh}} + \tau_{\text{d}} + \tau_{\text{ch}}, \quad (13)$$

where τ_{K} is Koehler stress originating from modulus mismatch, τ_{Ke} is the modification to Koehler stress due to

variation of elastic modulus in each layer [74], τ_{coh} is derived from coherency stress, τ_d is determined by misfit dislocations due to lattice mismatch, and τ_{ch} is the chemical interaction term related to stacking fault energy difference between constituent layers. The relative contribution of each term appearing in Eq. (13) has been studied for Cu/Ni and, to a lesser extent, Cu/Co, as discussed below.

Previously, modulus mismatch has been considered as a significant barrier to dislocation transmission. In an A/B system, since the energy/length of a dislocation is proportional to shear modulus μ, dislocations are attracted to reside in the lower modulus layer. As the influence of attractive or repulsive image force τ_K on dislocation is dependent on the difference in dislocation line energy between A and B layers, it is proportional to the modulus mismatch as [4,80]:

$$\tau_K = \frac{\mu_A(\mu_B - \mu_A)b\sin\theta}{4\pi(\mu_B + \mu_A)h}, \tag{14}$$

where θ is the smallest angle between the interface and glide planes. It becomes obvious from Eq. (14) that the magnitude of τ_K exhibits a significant dependence on h, being 0.002 GPa when $h = 100$ nm, but rising rapidly to 0.18 GPa when $h = 1$ nm for Cu/Ni. In addition, as predicted in Sect. 3.2, the elastic modulus is not a constant as h is varied and, further, τ_{Ke} is the modification to the Koehler stress. Atomistic simulations predict that the barrier due to modulus mismatch in Cu/Ni multilayers is 0.01μ, nearly independent of interface orientation and dislocation character [74]. When the layer thickness is reduced to a value comparable to dislocation core width, the Koehler stress may decrease considerably [74].

Lattice mismatch $\delta = \Delta a_0/a_0$ is another key parameter, which represents the level of elastic strain with respect to the stress-free reference state. The coherency stress is determined by lattice mismatch, though coherency is only likely for multilayers having small lattice mismatch. According to the coherent strain theory, the alternating compressive and tensile in-plane stress fields predicted by Eq. (2), which can inhibit dislocation motion, could lead to enhanced strength and hardness of multilayers. When a slip commences, it may be confined by oppositely signed compressive and tensile in-plane stresses in the adjoining layers. Macro-yielding is then expected when the applied stress is sufficient to eliminate the alternating signed stresses [74].

For multilayer systems having large lattice mismatch, the misfit is too large to achieve coherency in these systems, and hence misfit dislocations will be introduced to accommodate a portion of the misfit between the two constituent layers when h is larger than the critical layer thickness h_c for coherency loss. As a result, the interface barrier for multilayers with larger lattice mismatch is attributed to the spacing of misfit dislocations at the interface. Using atomic simulations, Hoagland et al. [75] examined slip behaviors in coherent and semi-coherent metallic bi-layered composites and concluded that semi-coherent interfaces could act as barriers to slip because of interaction between misfit and glide dislocations. Mathematically, the important role played by misfit dislocations in interface strengthening may be described as [128]:

$$\tau_d = \alpha\mu\left(\delta - \frac{b}{2h}\right), \tag{15}$$

where α is Saada's constant.

Chemical mismatch also contributes, though less significantly, to interface strength. As dislocation line energy tends to increase with SFE γ [129], a mismatch in γ can generate a force as the dislocation moves across an interface. In an A/B multilayer system, the chemical mismatch, τ_{ch}, arising from the SFE difference between A and B, may be approximated as [4,40]:

$$\tau_{ch} = \frac{\gamma_B - \gamma_A}{b}. \tag{16}$$

Incoherent interfaces are often present in non-isostructural fcc/bcc systems. Barriers to transmission of interfaces with weak bonding are typically caused by dislocation core delocalization and dislocation trapping in a low energy state (see Sect. 2.4). Transmission of such an interface requires compaction of dislocation core to nucleate a mobile dislocation in the adjacent crystal [77]. It is often believed that the strength displayed by an fcc/bcc interface tends to exceed that of an fcc/fcc interface, though opaque systems tend not to have large coherency stresses [130]. Incoherent interface barriers are often attributed to the low shear strength of interfaces and the resultant trapping of mobile dislocations [54]. Interfacial sliding generates an attractive force on mobile dislocations and allows for core spreading in the interface [53], thus hindering dislocation transmission. However, atomistic simulation results show that dislocation glide and climb at an interface may aid slip transmission [110,131]. In addition, while interfacial line defects (dislocations and disconnections) formed at an interface will interact with mobile dislocations to hinder successive interface slip on the same or adjacent slip systems in fcc/fcc NMMs, these will hardly work in fcc/bcc NMMs due to compaction of dislocation core.

4.2 Plastic instability

Deformation instability is a bifurcation of strains away from the uniform state. Localization of plastic strains is a common deformation-induced instability in NMMs. How it happens is related to both the microstructure and the way in which plasticity is mediated prior to localization. Generally, the ductility of NMMs is limited by the eventual formation of localized bands of intense plastic strain.
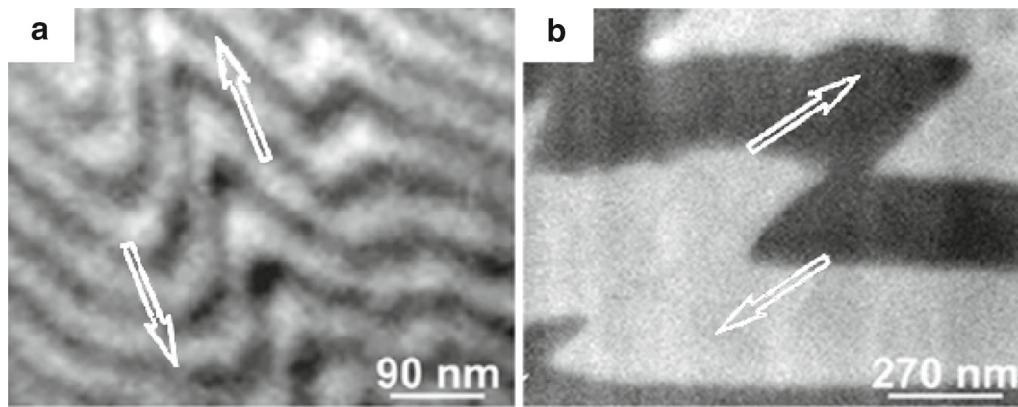
Fig. 13 Schematic illustration of two different deformation mechanisms corresponding to buckling-assisted layer rotation of **a** $h = 25$ nm multilayer and dislocation plasticity-dominated shearing of **b** $h = 250$ nm Au/Cu multilayer. Reprinted from Ref. [135] with permission

Shear banding has been extensively studied to reveal the mechanisms underlying inhomogeneous plastic deformation in nanocrystalline, amorphous solids and nanomultilayers. For NMMs, the formation of shear bands is attributed to diminished strain hardening ability and low strain rate sensitivity when the number of dislocations is limited and the mobility of interfaces increased. The hindered dislocation motion inside small grains is expected to make the interfaces more active to accommodate plastic deformation, resulting in interface-related deformation behaviors, such as grain rotation and grain boundary sliding. Works by Zhang et al. [132] and Wen et al. [35] revealed an increasing tendency of shear banding in nanometer-scale Cu/Au and Cu/Ag multilayers under indentation and attributed this phenomenon to the likely occurrence of grain boundary sliding.

Based on discussion presented in the previous sections, one can see clearly that individual layer thickness h is a key parameter to decide the mechanical properties of NMMs. Deformation instability (shear banding) is no exception. Experimental results of Au/Cu NMMs [132] demonstrate that when h falls within the nanometer regime, inhomogeneous shear banding becomes prevalent. Additionally, as h is reduced, the width of shear bands decreases while the maximum interface kink angle and pileup height increase [132–134]. Along with further microscopic observations, two different types of interface morphology have been identified as h is varied [5,6,135]: one is caused by layer rotation (Fig. 13a [135]), and the other arises from dislocations cutting across the interfaces (Fig. 13b [135]). The rotation and localization of strain within the shear band implies two competing layer-geometry-based mechanisms. At the nanometer scale, buckling-assisted GB sliding causes plastic instability of NMMs, while at the sub-micron (or larger) scale, dislocation plasticity dominates plastic instability [82].

For NMMs, another sound explanation of the length-scale-dependent shear banding behavior is the different mechanisms that control the deformation process [42,136].

When deformation is controlled by slip of single dislocations in confined layers, both constituent layers of a NMM can deform homogeneously and hence no shear band is formed. When h falls within the regime where there occur single dislocations cutting across interfaces, dislocation lines are not parallel across the hetero-interfaces, especially in fcc/bcc NMMs. As a result, crossing of single dislocations is difficult except in a particular slip system. When an indentor tip penetrates the multilayer system, the stress concentration thus induced can rotate the layers and, once an adequate amount of rotation has taken place, the particular slip system can be turned into an easy shear direction. As a result, shear instability may suddenly occur when the applied stress is greater than the critical value required for dislocation transmission in this direction [42].

5 Summary

The proliferation of publications on NMM thin films as a special class of structural composite materials is an indication of intense interest on this subject worldwide. In this survey, we have attempted to focus on the broad variation trends exhibited by the mechanical properties of NMMs, which may be rationalized using physically sound interface-related deformation mechanisms. Length scale and interface structure are widely considered two key factors dictating the mechanical performance of NMMs. Additionally, synthesis approach, testing method, grain size and morphology, and special microstructure such as twins and bubbles also play important roles in the unique strengthening and plastic deformation behavior of NMMs.

After all, the mechanical properties of NMMs are closely related to their microstructure, in particular, the interface structure. Understanding the interface and its deformation behavior holds the key to future development of high performance NMM systems, and controlling the microstructure

of NMMs can aid the design and manufacture of reliable multilayer systems and nanostructured composites. Abundant research opportunities exist in this area: in addition to the unresolved issues outlined in the present survey, the mechanics of creep, fatigue, fracture, and irradiation for multilayer systems is still in the early stage of data accumulation. An in-depth understanding of these issues will continue to be vigorously sought and, given the rapid development of relevant nanotechnology, appears to be in good sight.

References

1. Misra, A., Verdier, M., Lu, Y., et al.: Structure and mechanical properties of Cu–X (X = Nb, Cr, Ni) nanolayered composites. Scripta Materialia **39**, 555–560 (1998)
2. Clemens, B.M., Kung, H., Barnett, S.A.: Structure and strength of multilayers. MRS Bull. **24**, 20–26 (1999)
3. Misra, A., Kung, H., Embury, J.D.: Preface to the viewpoint set on: deformation and stability of nanoscale metallic multilayers. Scripta Materialia **50**, 707–710 (2004)
4. Bufford, D., Bi, Z., Jia, Q.X., et al.: Nanotwins and stacking faults in high-strength epitaxial Ag/Al multilayer films. Appl. Phys. Lett. **101**, 223112 (2012)
5. Mara, N.A., Bhattacharyya, D., Dickerson, P., et al.: Deformability of ultrahigh strength 5 nm Cu/Nb nanolayered composites. Appl. Phys. Lett. **92**, 231901 (2008)
6. Mara, N.A., Bhattacharyya, D., Dickerson, P., et al.: Ultrahigh strength and ductility of Cu–Nb nanolayered composites. Mater. Sci. Forum **633–634**, 647–653 (2009)
7. Misra, A., Zhang, X., Hammon, D., et al.: Work hardening in rolled nanolayered metallic composites. Acta Materialia **53**, 221–226 (2005)
8. Zhang, J.Y., Zhang, X., Wang, R.H., et al.: Length-scale-dependent deformation and fracture behavior of Cu/X (X = Nb, Zr) multilayers: the constraining effects of the ductile phase on the brittle phase. Acta Materialia **59**, 7368–7379 (2011)
9. Demkowicz, M.J., Hoagland, R.G., Hirth, J.P.: Interface structure and radiation damage resistance in Cu–Nb multilayer nanocomposites. Phys. Rev. Lett. **100**, 136102 (2008)
10. Han, W.Z., Demkowicz, M.J., Mara, N.A., et al.: Design of radiation tolerant materials via interface engineering. Adv. Mater. **25**, 6975–6979 (2013)
11. Hattar, K., Demkowicz, M.J., Misra, A., et al.: Arrest of He bubble growth in Cu–Nb multilayer nanocomposite. Scripta Materialia **58**, 541–544 (2008)
12. Li, N., Nastasi, M., Misra, A.: Defect structures and hardening mechanisms in high dose helium ion implanted Cu and Cu/Nb multilayer thin films. Int. J. Plast. **32–33**, 1–16 (2012)
13. Han, W.Z., Misra, A., Mara, N.A., et al.: Role of interfaces in shock-induced plasticity in Cu/Nb nanolaminates. Philos. Mag. **91**, 4172–4185 (2011)
14. Han, W.Z., Cerreta, E.K., Mara, N.A., et al.: Deformation and failure of shocked bulk Cu–Nb nanolaminates. Acta Materialia **63**, 150–161 (2014)
15. Misra, A., Hoagland, R.G.: Effects of elevated temperature annealing on the structure and hardness of copper/niobium nanolayered films. J. Mater. Res. **20**, 2046–2054 (2005)
16. Zheng, S., Beyerlein, I.J., Carpenter, J.S., et al.: High-strength and thermally stable bulk nanolayered composites due to twin-induced interfaces. Nat. Commun. **4**, 1696 (2013)
17. Wen, S.P., Zong, R.L., Zeng, F., et al.: Thermal stability of microstructure and mechanical properties of Ni/Ru multilayers. Surf. Coat. Technol. **202**, 2040–2046 (2008)
18. Dew-Hughes, D.: High strength conductor for pulsed magnets. Mater. Sci. Eng. A **168**, 35–40 (1993)
19. Freudenberger, J., Grunberger, W., Botcharova, E., et al.: Mechanical properties of Cu-based micro- and macrocomposites. Adv. Eng. Mater. **4**, 677–681 (2002)
20. Sandim, M.J.R., Stamopoulos, D., Ghivelder, L., et al.: Paramagnetic meissner effect and AC magnetization in roll-bonded Cu–Nb layered composites. J. Superconduct. Novel Magn. **23**, 1533–1541 (2010)
21. Beyerlein, I.J., Wang, J., Zhang, R.: Mapping dislocation nucleation behavior from bimetal interfaces. Acta Materialia **61**, 7488–7499 (2013)
22. Mara, N.A., Beyerlein, I.J.: Review: effect of bimetal interface structure on the mechanical behavior of Cu–Nb fcc–bcc nanolayered composites. J. Mater. Sci. **49**, 6497–6516 (2014)
23. Zhou, Q., Wang, F., Huang, P., et al.: Strain rate sensitivity and related plastic deformation mechanism transition in nanoscale Ag/W multilayers. Thin Solid Films **571**, 253–259 (2014)
24. Geng, H.: Semiconductor Manufacturing Handbook, 1st edn. McGraw-Hill Professional, Blacklick (2005)
25. Thompson, C.V.: Grain-growth in thin-films. Annu. Rev. Mater. Sci. **20**, 245–268 (1990)
26. Thompson, C.V.: Structure evolution during processing of polycrystalline films. Annu. Rev. Mater. Sci. **30**, 159–190 (2000)
27. Wei, Q., Misra, A.: Transmission electron microscopy study of the microstructure and crystallographic orientation relationships in V/Ag multilayers. Acta Materialia **58**, 4871–4882 (2010)
28. Chirranjeevi, B.G., Abinandanan, T.A., Gururajan, M.P.: A phase field study of morphological instabilities in multilayer thin films. Acta Materialia **57**, 1060–1067 (2009)
29. Bakonyi, I., Peter, L.: Electrodeposited multilayer films with giant magnetoresistance (GMR): progress and problems. Prog. Mater. Sci. **55**, 107–245 (2010)
30. Yahalom, J., Tessier, D.F., Timsit, R.S., et al.: Structure of composition-modulated Cu/Ni thin-films prepared by electrodeposition. J. Mater. Res. **4**, 755–758 (1989)
31. Haseeb, A.S.M.A., Celis, J.P., Roos, J.R.: Dual-bath electrodeposition of Cu/Ni compositionally modulated multilayers. J. Electrochem. Soc. **141**, 230–237 (1994)
32. Toth-Kadar, E., Peter, L., Becsei, T., et al.: Preparation and magnetoresistance characteristics of electrodeposited Ni–Cu alloys and Ni–Cu/Cu multilayers. J. Electrochem. Soc. **147**, 3311–3318 (2000)
33. Wen, S.P., Zeng, F., Pan, F., et al.: The influence of grain morphology on indentation deformation characteristic of metallic nano-multilayers. Mater. Sci. Eng. A **526**, 166–170 (2009)
34. Wen, S.P., Zeng, F., Gao, Y., et al.: Indentation creep behavior of nano-scale Ag/Co multilayers. Scripta Materialia **55**, 187–190 (2006)
35. Wen, S.P., Zong, R.L., Zeng, F., et al.: Nanoindentation investigation of the mechanical behaviors of nanoscale Ag/Cu multilayers. J. Mater. Res. **22**, 3423–3431 (2007)
36. Wen, S.P., Zong, R.L., Zeng, F., et al.: Evaluating modulus and hardness enhancement in evaporated Cu/W multilayers. Acta Materialia **55**, 345–351 (2007)

37. Wen, S.P., Zong, R.L., Zeng, F., et al.: Nanoindentation and nano-scratch behaviors of Ag/Ni multilayers. Appl. Surf. Sci. **255**, 4558–4562 (2009)

38. Zhu, X.Y., Liu, X.J., Zong, R.L., et al.: Microstructure and mechanical properties of nanoscale Cu/Ni multilayers. Mater. Sci. Eng. A **527**, 1243–1248 (2010)

39. Liu, Y., Bufford, D., Wang, H., et al.: Mechanical properties of highly textured Cu/Ni multilayers. Acta Materialia **59**, 1924–1933 (2011)

40. Liu, Y., Chen, Y., Yu, K.Y., et al.: Stacking fault and partial dislocation dominated strengthening mechanisms in highly textured Cu/Co multilayers. Int. J. Plast. **49**, 152–163 (2013)

41. Zhu, X.Y., Luo, J.T., Chen, G., et al.: Size dependence of creep behavior in nanoscale Cu/Co multilayer thin films. J. Alloys Compd. **506**, 434–440 (2010)

42. Zhu, X.Y., Luo, J.T., Zeng, F., et al.: Microstructure and ultrahigh strength of nanoscale Cu/Nb multilayers. Thin Solid Films **520**, 818–823 (2011)

43. Wang, F., Zhang, L.F., Huang, P., et al.: Microstructure and flow stress of nanoscale Cu/Nb multilayers. J. Nanomater. (2013). doi:10.1155/2013/912548

44. Bauer, E., Merwe, J.H.V.D.: Structure and growth of crystalline superlattices: from monolayer to superlattice. Phys. Rev. B **33**, 3657–3671 (1986)

45. Zhou, Q., Li, Y., Wang, F., et al.: Length-scale-dependent mechanical properties of Cu/Ru multilayer films: Part I. Microstructure and strengthening mechanisms. (To be submitted to Acta Mater.)

46. Lewis, A.C., Josell, D., Weihs, T.P.: Stability in thin film multilayers and microlaminates: the role of free energy, structure, and orientation at interfaces and grain boundaries. Scripta Materialia **48**, 1079–1085 (2003)

47. Misra, A., Hoagland, R.G., Kung, H.: Thermal stability of self-supported nanolayered Cu/Nb films. Philos. Mag. **84**, 1021–1028 (2004)

48. Wan, H., Shen, Y., Wang, J., et al.: A predictive model for microstructure evolution in metallic multilayers with immiscible constituents. Acta Materialia **60**, 6869–6881 (2012)

49. Beyerlein, I.J., Mara, N.A., Wang, J., et al.: Structure–property–functionality of bimetal interfaces. JOM **64**, 1192–1207 (2012)

50. Kang, K., Wang, J., Beyerlein, I.J.: Atomic structure variations of mechanically stable fcc–bcc interfaces. J. Appl. Phys. **5**, 053531 (2012)

51. Wang, J., Hoagland, R.G., Misra, A.: Mechanics of nanoscale metallic multilayers: from atomic-scale to micro-scale. Scripta Materialia **60**, 1067–1072 (2009)

52. Wang, J., Hoagland, R.G., Hirth, J.P., et al.: Atomistic modeling of the interaction of glide dislocations with "weak" interfaces. Acta Materialia **56**, 5685–5693 (2008)

53. Wang, J., Hoagland, R.G., Hirth, J.P., et al.: Atomistic simulations of the shear strength and sliding mechanisms of copper–niobium interfaces. Acta Materialia **56**, 3109–3119 (2008)

54. Hoagland, R.G., Kurtz, R.J., Henager Jr, C.H.: Slip resistance of interfaces and the strength of metallic multilayer composites. Scripta Materialia **50**, 775–779 (2004)

55. Beyerlein, I.J., Wang, J., Zhang, R.: Interface-dependent nucleation in nanostructured layered composites. APL Mater. **1**, 032112 (2013)

56. Zhang, R.F., Wang, J., Beyerlein, I.J., et al.: Atomic-scale study of nucleation of dislocations from fcc–bcc interfaces. Acta Materialia **60**, 2855–2865 (2012)

57. Kulkarni, Y., Asaro, R.J.: Are some nanotwinned fcc metals optimal for strength, ductility and grain stability? Acta Materialia **57**, 4835–4844 (2009)

58. Zhang, X., Misra, A., Wang, H., et al.: Nanoscale-twinning-induced strengthening in austenitic stainless steel thin films. Appl. Phys. Lett. **84**, 1096–1098 (2004)

59. Lu, L., Shen, Y.F., Chen, X.H., et al.: Ultrahigh strength and high electrical conductivity in copper. Science **304**, 422–426 (2004)

60. Zhang, X., Misra, A.: Superior thermal stability of coherent twin boundaries in nanotwinned metals. Scripta Materialia **66**, 860–865 (2012)

61. Anderoglu, O., Misra, A., Wang, J., et al.: Plastic flow stability of nanotwinned Cu foils. Int. J. Plast. **26**, 875–886 (2010)

62. Li, N., Wang, J., Misra, A., et al.: Twinning dislocation multiplication at a coherent twin boundary. Acta Materialia **59**, 5989–5996 (2011)

63. Lu, L., Shen, Y.F., Dao, M., et al.: Strain rate sensitivity of Cu with nanoscale twins. Scripta Materialia **55**, 319–322 (2006)

64. Liu, Y., Bufford, D., Rioset, S., et al.: A formation mechanism for ultra-thin nanotwins in highly textured Cu/Ni multilayers. J. Appl. Phys. **111**, 073526 (2012)

65. Bufford, D., Liu, Y., Zhu, Y., et al.: Formation mechanisms of high-density growth twins in aluminum with high stacking-fault energy. Mater. Res. Lett. **1**, 51–60 (2013)

66. Freund, L.B., Suresh, S.: Thin Film Materials: Stress, Defect Formation and Surface Evolution. Cambridge University Press, Cambridge (2004)

67. Mata, M., Anglada, M., Alcala, J.: Contact deformation regimes around sharp indentations and the concept of the characteristic strain. J. Mater. Res. **17**, 964–976 (2002)

68. Blum, W.: The structure and properties of alternately deposited metals. Trans. Am. Electrochem. Soc. **40**, 307–320 (1921)

69. Misra, A., Hirth, J.P., Kung, H.: Single-dislocation-based strengthening mechanisms in nanoscale metallic multilayers. Philos. Mag. A **82**, 2935–2951 (2002)

70. Tench, D.M., White, J.T.: Tensile properties of nanostructured Ni–Cu multilayered materials prepared by electrodeposition. J. Electrochem. Soc. **138**, 3757–3758 (1991)

71. Carpenter, J.S., Misra, A., Uchic, M.D., et al.: Strain rate sensitivity and activation volume of Cu/Ni metallic multilayer thin films measured via micropillar compression. Appl. Phys. Lett. **101**, 051901 (2012)

72. Carpenter, J.S., Misra, A., Anderson, P.M.: Achieving maximum hardness in semi-coherent multilayer thin films with unequal layer thickness. Acta Materialia **60**, 2625–2636 (2012)

73. Cammarata, R.C., Schlesinger, T.E., Kim, C., et al.: Nanoindentation study of the mechanical-properties of cppper–nickel multilayered thin-films. Appl. Phys. Lett. **56**, 1862–1864 (1990)

74. Rao, S.I., Hazzledine, P.M.: Atomistic simulations of dislocation–interface interactions in the Cu–Ni multilayer system. Philos. Mag. A **80**, 2011–2040 (2000)

75. Hoagland, R.G., Mitchell, T.E., Hirth, J.P., et al.: On the strengthening effects of interfaces in multilayer fcc metallic composites. Philos. Mag. A **82**, 643–664 (2002)

76. Misra, A., Hirth, J.P., Hoagland, R.G.: Length-scale-dependent deformation mechanisms in incoherent metallic multilayered composites. Acta Materialia **53**, 4817–4824 (2005)

77. Zhang, J.Y., Zhang, P., Zhang, X., et al.: Mechanical properties of fcc/fcc Cu/Nb nanostructured multilayers. Mater. Sci. Eng. A **545**, 118–122 (2012)

78. Mara, N.A., Bhattacharyya, D., Hoagland, R.G., et al.: Tensile behavior of 40 nm Cu/Nb nanoscale multilayers. Scripta Materialia **58**, 874–877 (2008)

79. Fu, E.G., Li, N., Misra, A., et al.: Mechanical properties of sputtered Cu/V and Al/Nb multilayer films. Mater. Sci. Eng. A **493**, 283–287 (2008)

80. Koehler, J.: Attempt to design a strong solid. Phys. Rev. B **2**, 547–551 (1970)

81. Akcakaya, E., Famell, G.W., Adler, E.L.: Dynamic approach for finding effective elastic and piezoelectric constants of superlattices. J. Appl. Phys. **68**, 1009 (1990)

82. Li, Y.P., Zhu, X.F., Zhang, G.P., et al.: Investigation of deformation instability of Au/Cu multilayers by indentation. Philos. Mag. **90**, 3049–3067 (2010)

83. Chen, Y., Liu, Y., Sun, C., et al.: Microstructure and strengthening mechanisms in Cu/Fe multilayers. Acta Materialia **60**, 6312–6321 (2012)

84. Huang, P., Wang, F., Xu, M., et al.: Strain rate sensitivity of unequal grained nano-multilayers. Mater. Sci. Eng. A **528**, 5908–5913 (2011)

85. Zhang, J.Y., Liu, Y., Chen, J., et al.: Mechanical properties of crystalline Cu/Zr and crystal–amorphous Cu/Cu–Zr multilayers. Mater. Sci. Eng. A **552**, 392–398 (2012)

86. Hu, K., Xu, L.J., Cao, Y.Q., et al.: Modulating individual thickness for optimized combination of strength and ductility inCu/Ru multilayer films. Mater. Lett. **107**, 303–306 (2013)

87. Lai, W.S., Yang, M.J.: Observation of largely enhanced hardness in nanomultilayers of the Ag–Nb system with positive enthalpy of formation. Appl. Phys. Lett. **90**, 181917 (2007)

88. Wen, S.P., Zeng, F., Gao, Y., et al.: Microstructure and nanoindentation investigation of magnetron sputtering Ag/Co multilayers. Surf. Coat. Technol. **201**, 1262–1266 (2006)

89. Wen, S.P., Zong, R.L., Zeng, F., et al.: Influence of plasticity mismatch and porosity on mechanical behavior of nanoscale Ag/W multilayers. Mater. Sci. Eng. A **457**, 38–43 (2007)

90. Abadias, G., Jaouen, C., Martin, F., et al.: Experimental evidence for the role of supersaturated interfacial alloys on the shear elastic softening of Ni/Mo superlattices. Phys. Rev. B **65**, 212105 (2002)

91. Zhang, J.Y., Niu, J.J., Zhang, X., et al.: Tailoring nanostructured Cu/Cr multilayer films with enhanced hardness and tunable modulus. Mater. Sci. Eng. A **543**, 139–144 (2012)

92. Huang, H., Spaepen, F.: Tensile testing of free-standing Cu, Ag and Al thin films and Ag/Cu multilayers. Acta Materialia **48**, 3261–3269 (2000)

93. Zhang, J.Y., Lei, S., Liu, Y., et al.: Length scale-dependent deformation behavior of nanolayered Cu/Zr micropillars. Acta Materialia **60**, 1610–1622 (2012)

94. Mara, N.A., Bhattacharyya, D., Hirth, J.P., et al.: Mechanism for shear banding in nanolayered composites. Appl. Phys. Lett. **97**, 021909 (2010)

95. Carpenter, J.S., Vogel, S.C., LeDonne, J.E., et al.: Bulk texture evolution of Cu–Nb nanolamellar composites during accumulative roll bonding. Acta Materialia **60**, 1576–1586 (2012)

96. Anderson, P.M., Bingert, J.F., Misra, A., et al.: Rolling textures in nanoscale Cu/Nb multilayers. Acta Materialia **51**, 6059–6075 (2003)

97. Misra, A., Kung, H., Hammon, D., et al.: Damage mechanisms in nanolayered metallic composites. Int. J. Damage Mech. **12**, 365–376 (2003)

98. Hsia, K.J., Suo, Z., Yang, W.: Cleavage due to dislocation confinement in layered materials. J. Mech. Phys. Solids **42**, 877–896 (1994)

99. Was, G.S., Foecke, T.: Deformation and fracture in microlaminates. Thin Solid Films **286**, 1–31 (1996)

100. Hertzberg, R.W.: Deformation and Fracture Mechanics of Engineering Materials. Wiley, New York (1989)

101. Zhang, J.Y., Liu, G., Sun, J., et al.: Dominant factor controlling the fracture mode in nanostructured Cu/Cr multilayer films. Mater. Sci. Eng. A **528**, 2982–2987 (2011)

102. Zhou, Q., Zhao, J., Xie, J.Y., et al.: Grain size dependent strain rate sensitivity in nanocrystalline body-centered cubic metal thin films. Mater. Sci. Eng. A **608**, 184–189 (2014)

103. Lu, L., Schwaiger, R., Shan, Z.W., et al.: Nano-sized twins induce high rate sensitivity of flow stress in pure copper. Acta Materialia **53**, 2169–2179 (2005)

104. Schwaiger, R., Moser, B., Dao, M., et al.: Some critical experiments on the strain-rate sensitivity of nanocrystalline nickel. Acta Materialia **51**, 5159–5172 (2003)

105. Wei, Q., Cheng, S., Ramesh, K.T., et al.: Effect of nanocrystalline and ultrafine grain sizes on the strain rate sensitivity and activation volume: fcc versus bcc metals. Mater. Sci. Eng. A **381**, 71–79 (2004)

106. Wang, F., Li, B., Gao, T.T., et al.: Activation volume and strain rate sensitivity in plastic deformation of nanocrystalline Ti. Surf. Coat. Technol. **228**, S254–S256 (2012)

107. Niu, J.J., Zhang, J.Y., Liu, G., et al.: Size-dependent deformation mechanisms and strain-rate sensitivity in nanostructured Cu/X (X = Cr, Zr) multilayer films. Acta Materialia **60**, 3677–3689 (2012)

108. Zhu, X.Y., Liu, X.J., Zeng, F., et al.: Room temperature nanoindentation creep of nanoscale Ag/Fe multilayers. Mater. Lett. **64**, 53–56 (2010)

109. Shen, B.L., Itoi, T., Yamasaki, T., et al.: Indentation creep of nanocrystalline Cu–TiC alloys prepared by mechanical alloying. Scripta Materialia **42**, 893–898 (2000)

110. Wang, J., Hoagland, R.G., Misra, A.: Room-temperature dislocation climb in metallic interfaces. Appl. Phys. Lett. **94**, 131910 (2009)

111. Kang, B.C., Kim, H.Y., Kwon, O.Y., et al.: Bilayer thickness effects on nanoindentation behavior of Ag/Ni multilayers. Scripta Materialia **57**, 703–706 (2007)

112. Zhang, J.Y., Wang, Y.Q., Wu, K., et al.: Strain rate sensitivity of nanolayered Cu/X (X = Cr, Zr) micropillars: effects of heterophase interface/twin boundary. Mater. Sci. Eng. A **61**, 228–240 (2014)

113. Friedman, L.H., Chrzan, D.C.: Scaling theory of the Hall–Petch relation for multilayers. Phys. Rev. Lett. **81**, 2715–2718 (1998)

114. Embury, J.D., Hirth, J.P.: On dislocation storage and the mechanical response of fine scale microstructures. Acta Metallurgica et Materialia **42**, 2051–2056 (1994)

115. Anderson, P.M., Foecke, T., Hazzledine, P.M.: Dislocation-based deformation mechanisms in metallic nanolaminates. MRS Bull. **24**, 27–33 (1999)

116. Wang, J., Misra, A.: Strain hardening in nanolayered thin films. Curr. Opin. Solid State Mater. Sci. **18**, 19–28 (2014)

117. Kramer, D.E., Foecke, T.: Transmission electron microscopy observations of deformation and fracture in nanolaminated Cu–Ni thin films. Philos. Mag. A **82**, 3375–3381 (2002)

118. Tu, K., Mayer, J.W., Feldman, L.C.: Electronic Thin Film Science: for Electrical Engineers and Materials Scientists. Macmillan, New York (1992)

119. Misra, A., Verdier, M., Kung, H., et al.: Deformation mechanism maps for polycrystalline metallic multiplayers. Scripta Materialia **41**, 973–979 (1999)

120. Yan, J.W., Zhu, X.F., Zhang, G.P., et al.: Evaluation of plastic deformation ability of Cu/Ni/W metallic multilayers. Thin Solid Films **527**, 227–231 (2013)

121. Kamat, S.V., Hirth, J.P.: Dislocation injection in strained multilayer structures. J. Appl. Phys. **67**, 6844–6850 (1990)

122. Mastorakos, I.N., Zbib, H.M., Bahr, D.F.: Deformation mechanisms and strength in nanoscale multilayer metallic composites with coherent and incoherent interfaces. Appl. Phys. Lett. **94**, 173114 (2009)

123. Lehoczky, S.L.: Strength enhancement in thin-layered Al–Cu laminates. J. Appl. Phys. **49**, 5479–5485 (1978)

124. Shinn, M., Hultman, L., Barnett, S.A.: Growth, structure, and microhardness of epitaxial TlN/NBN superlattices. J. Mater. Res. **7**, 901–911 (1992)

125. Xu, J.H., Kamiko, M., Sawada, H., et al.: Structure, hardness, and elastic modulus of Pd/Ti nanostructured multilayer films. J. Vac. Sci. Technol. B **21**, 2584–2589 (2003)

126. Li, Y.P., Zhang, G.P., Wang, W.: On interface strengthening ability in metallic multilayers. Scripta Materialia **57**, 117–120 (2007)

127. Kim, C., Qadri, S.B., Scanlon, M.R., et al.: Low-dimension structural properties and microindentation studies of ion-beam-sputtered multilayers of Ag/Al films. Thin Solid Films **240**, 52–55 (1994)

128. Lu, Y.Y., Kotoka, R., Ligda, J.P., et al.: The microstructure and mechanical behavior of Mg/Ti multilayers as a function of individual layer thickness. Acta Materialia **63**, 216–231 (2014)

129. Hirth, J.P., Lothe, J.: Theory of Dislocations. Krieger, Malabar (1992)

130. Wang, J., Hoagland, R.G., Misra, A.: Phase transition and dislocation nucleation in Cu–Nb layered composites during physical vapor deposition. J. Mater. Res. **23**, 1009–1014 (2008)

131. Zhang, R.F., Wang, J., Beyerlein, I.J., et al.: Dislocation nucleation mechanisms from fcc/bcc incoherent interfaces. Scripta Materialia **65**, 1022–1025 (2011)

132. Zhang, G.P., Liu, Y., Wang, W., et al.: Experimental evidence of plastic deformation instability in nanoscale Au/Cu multilayers. Appl. Phys. Lett. **88**, 013105 (2006)

133. Li, Y.P., Tan, J., Zhang, G.P.: Interface instability within shear bands in nanoscale Au/Cu multilayers. Scripta Materialia **59**, 1226–1229 (2008)

134. Xie, J.Y., Huang, P., Wang, F., et al.: Shear banding behavior in nanoscale Al/W multilayers. Surf. Coat. Technol. **228**, S593–S596 (2013)

135. Li, Y.P., Zhu, X.F., Tan, J., et al.: Two different types of shear-deformation behaviour in Au–Cu multilayers. Philos. Mag. Lett. **89**, 66–74 (2009)

136. Bhattacharyya, D., Mara, N.A., Dickerson, P., et al.: Transmission electron microscopy study of the deformation behavior of Cu/Nb and Cu/Ni nanoscale multilayers during nanoindentation. J. Mater. Res. **24**, 1291–1302 (2009)